Journal of Membrane Science 690 (2024) 122226

Contents lists available at ScienceDirect

Journal of Membrane Science

journal homepage: www.elsevier.com/locate/memsci

Fabrication and characterization of coated ceramic membranes from natural sources for water treatment applications

Mohammed D. Alsubei [a,d], Barry Reid [b], Saad A. Aljlil [c], Marc-Olivier Coppens [b], Luiza C. Campos [a,*]

[a] Centre for Urban Sustainability and Resilience, Department of Civil, Environmental and Geomatic Engineering, University College London, Gower Street, London, WC1E 6BT, UK
[b] Department of Chemical Engineering &Centre for Nature-Inspired Engineering, University College London, London, WC1E 7JE, UK
[c] Water Management and Treatment Technologies Institute, King Abdulaziz City for Science and Technology, P.O. Box 6086, Riyadh, 11442, Saudi Arabia
[d] Desalination Technology Institute, King Abdulaziz City for Science and Technology, P.O. Box 6086, Riyadh, 11442, Saudi Arabia

ARTICLE INFO

Keywords:
Ceramic membrane
White clay
Silica flour
Marble powder
Water treatment applications

ABSTRACT

This study aimed to fabricate ceramic membranes for water treatment applications using natural and cost-effective materials. This is the first-time white clay, Arabic gum, and marble powder were used in ceramic membranes. Two ceramic membranes were fabricated using an extrusion process: substrate A and substrate B. The JMP software (Version 15) was used to obtain the optimal recipes for the two substrates, which were white clay (62.7 %), silica flour (32.3 %), and Arabic gum (5 %) for substrate A and white clay (63 %), silica flour (26.8 %), and marble powder (10.2 %) for substrate B. Additionally, the effect of waste glass in the coating layer on the separation rate was examined. The ceramic membranes were analysed using various techniques, including X-ray fluorescence (XRF), X-ray diffraction (XRD), Fourier-transform infrared spectroscopy (FT-IR), laser diffraction particle size analysis, thermogravimetric analysis (TGA), and a universal testing machine. The morphologies of the membranes were observed using scan electron microscopy (SEM), and their chemical resistances were evaluated. The flux across the substrates was measured using a crossflow filtration system, and it was found that substrate B had a higher flux (116 L/m^{2}h) than substrate A (77 L/m^{2}h). This was probably due to its higher porosity (34 %) compared to substrate A (29 %). Substrate A, with a coating layer (CO-2), exhibited the highest removal efficiency of approximately 99.2 % for synthetic feed water composed of tap water and bentonite clay, with an average particle size of 1.1 μm and turbidity of 13 ± 0.2 NTU. The costs of ceramic membranes A and B were estimated to be approximately 51 and 47 USD/m^2, respectively. Their cost-effectiveness results from the use of low-cost materials that do not require high sintering temperatures. This study demonstrates that these ceramic membranes are not only affordable but also possess desirable properties for water treatment applications.

1. Introduction

The demand for water treatment has increased significantly in recent years and is likely to continue in the coming decades. Several factors contribute to this increased demand, including global environmental changes, population growth, industrialisation, and urbanisation. Consequently, researchers, companies, and governments will pay more attention to developing appropriate water treatment technologies.

The use of membrane technology in water treatment has grown significantly, with polymeric membranes being commonly applied for reverse osmosis desalination to remove dissolved mineral salts. Ceramic membranes are preferred for ultrafiltration and microfiltration because of their properties [1], including better thermal and chemical stability and less fouling potential [2–4].

They can be synthesised using various materials such as alumina, titania, zirconia, and silica [5] and these expensive materials have been used in the earlier fabrication stages [6–8]. Conventional ceramic membranes cost between 500 and 3000 USD/m^2 [9]. The use of such expensive materials may be attributed to their reliability, stability, and robustness. However, there is an increasing demand for low-cost materials that can compete with expensive materials by providing similar features, particularly in lower/middle-income countries, where

* Corresponding author.
E-mail address: l.campos@ucl.ac.uk (L.C. Campos).

https://doi.org/10.1016/j.memsci.2023.122226
Received 6 September 2023; Received in revised form 26 October 2023; Accepted 30 October 2023
Available online 2 November 2023

importing technology is difficult owing to a lack of resources.

Recently, many researchers have focused on utilising less expensive materials such as natural clay [10] in the production of ceramic membranes. It is also possible to reduce the cost of membranes by using low-cost materials for the substrate and intermediate layers, as demonstrated by Chougui et al. [11]. Barbotine, a kaolin, and zirconia mixture (3 %) were used as the substrate and intermediate layers, respectively, whereas 3-mercaptopropyltrimethyoxysilane was used as a filtering layer, which was prepared using the sol-gel technique. However, identifying suitable naturally available materials for fabricating ceramic membranes requires intensive investigation because using one type of natural material may not provide the desired ceramic membrane properties, such as high flux and stable structure. Mixtures of two or more natural materials may provide better ceramic membrane characteristics. Moreover, finding the optimal mixture percentage of different ingredients can enhance the thermal and chemical stability of the ceramic membrane with good permeability and separation properties [12].

In the fabrication of ceramic membranes, prior knowledge of the effect of additives on ceramic properties is crucial. However, selecting a particular additive to improve membrane performance is challenging because multiple variables affect the final product. Nandi et al. [12] reported a low-cost (USD130/m^2) ceramic membrane for microfiltration applications made of low-cost materials, such as kaolin (40 wt %), quartz (15 wt%), calcium carbonate (25 wt%), sodium carbonate (10 wt %), and other additives such as boric acid (5 wt%) and sodium metasilicate (5 wt%). Kaolin provides membranes with low plasticity and high refractory properties, whereas quartz increases their mechanical and thermal stability. Calcium carbonate is used as a pore-forming agent, because it decomposes into CaO and CO_2 during the sintering process. Sodium carbonate can also act as a colloidal agent. Boric acid has two functions: (1) increasing the membrane strength by forming metallic metaborates at sintering temperatures, and (2) acting as a colloidal agent, improving the dispersion properties of inorganic precursors, and ensuring homogeneity in the membrane structure. However, these authors did not report the method used to determine the optimal percentage of each component.

Moreover, using an appropriate particle-size distribution can improve the stability of the substrate and prevent the formation of holes in its structure. Reed [13] reported that flow resistance decreased as the particle size decreased.

Even though ceramic membranes have attracted significant attention for their potential applications in water treatment due to their superior mechanical, thermal, and chemical stability, the high cost of production and the limited availability of raw materials have hindered their commercialization [14]. Our work offers several innovative aspects that help to overcome the previous issues. Therefore, the aim of this study was to develop an optimal ceramic membrane using natural and cost-effective materials. This is the first-time that white clay, Arabic gum, and marble powder were used to fabricate ceramic membranes for water treatment applications. Incorporating waste glass into the coating layer adds a sustainable dimension by reusing materials to enhance membrane performance. In addition, the combination of materials may contribute to forming a more stable and robust structure of ceramic membranes. Finally, a cost analysis was conducted to determine the cost-effectiveness of the membranes and compare them to similar products.

2. Materials and methods

2.1. Raw materials

This study utilised four natural materials to produce two ceramic membrane substrates, called substrate A and substrate B. Substrate A comprised white clay, silica flour, and Arabic gum, whereas substrate B was composed of white clay, silica flour, and marble powder. The coating layer for both substrates was a mixture of white clay, waste glass, and Arabic gum.

White clay was collected from Jalajil, northern Riyadh, Saudi Arabia. Silica flour was obtained from Adwan Chemical Industries Co. Ltd., and Arabic gum was purchased from a local market in Riyadh, Saudi Arabia. Marble powder was purchased from the BMS Gharbalah Industrial Company. Before use, some materials, such as white clay, Arabic gum, and waste glass, were ground and sieved. The chemical composition, particle size distribution, and thermal properties are presented in Section 3.

2.2. Preparation of the ceramic membranes

A simple approach was used to fabricate ceramic membranes, including the preparation of ceramic substrates and coating of the inner substrate surface using the dip-coating technique.

2.2.1. Preparation of the ceramic substrates

The fabrication of ceramic substrates involves various steps, including grinding and sieving, batching, mixing, extrusion, drying, and sintering. The raw materials, such as white clay that needed to be ground, were crushed using a Fritsch disc mill (Pulverisette 13, Germany) and then sieved to obtain the desired particle size using a sieve shaker (Humboldt, USA). In the batching step, the JMP software was used to design the experimental recipes, as shown in Table 1.

To prepare the paste for every batch, specific amounts of raw materials were weighed according to the batch composition listed in Table 1, and mixed using a roller mixer for 30 min. Following dry mixing, the intended quantity of water (20–25 % relative to the total mass i.e. the water and solid mixture) was gradually introduced into the high-speed mixer during the wet-mixing stage. In the initial stages, half of the desired amount of water was added to the mixer by spraying and mixing for 5 min, followed by the remaining half. When the paste's plasticity was satisfactory, a mixture or dough was formed with minimal paste sticking to the inner wall of the high-speed mixer. The paste was subsequently extruded and allowed to dry in open air for several days, using wooden grooves covered in plastic film. During this time, the tubes were periodically turned, and water drops were removed to prevent condensation. The drying process continued until the surface appeared dry, with a noticeable change in colour and texture, signifying that it had become harder. Sintering of the produced substrates was performed by heating the substrates to a temperature below the melting point until the particles of the different materials fused and consolidated. In this study, sintering was performed in three steps. First, the substrate was heated to 100 °C at a rate of 2 °C/min to eliminate any residual moisture. Second, substrate A, which contained Arabic gum, was heated from 100 °C to 500 °C at a rate of 5 °C/min. In contrast, substrate B was heated from 100 °C to 800 °C at a rate of 5 °C/min because marble powder contains more than 96 % of calcium carbonate, which decomposes to CaO and CO_2 at 800 °C. Third, the ceramic network was densified by sintering at

Table 1
Batch compositions generated by the JMP software.

Number	Substrate A			Substrate B		
	White clay (%)	Silica flour (%)	Arabic gum (%)	White clay (%)	Silica flour (%)	Marble powder (%)
1	85	10	5	50	45	5
2	50	45	5	70	10	20
3	67.5	27.5	5	85	10	5
4	57.5	17.5	25	50	30	20
5	50	33.65	16.34			
6	50	25	25			
7	62.5	22.13	15.32			
8	65	10	25			
9	73.35	10	16.65			

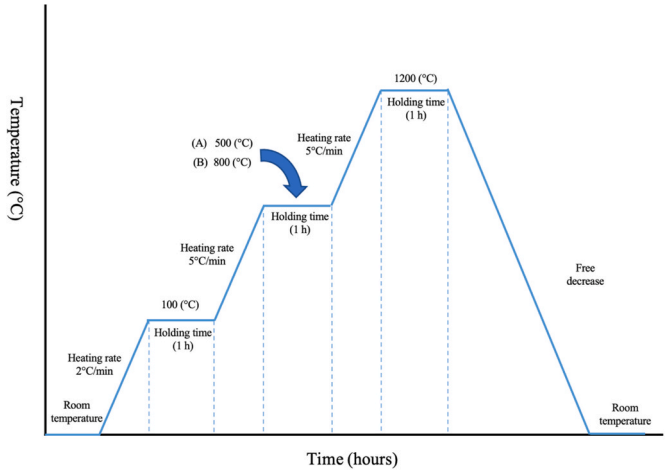

Fig. 1. Thermal treatment programs (A or B) used for substrate sintering.

500 °C–1200 °C at a rate of 5 °C/min. The substrates were placed horizontally in an electric furnace (LH216/12; Nebertherm, Germany) and combusted under normal atmospheric conditions. Fig. 1 shows the thermal treatment programs when the temperatures during the second step were (A) 500 °C or (B) 800 °C.

2.2.2. Preparation of slurry for the coating layer

For slurry preparation, the feed particles, which were ground using a Fritsch disc mill (Pulverisette 13, Germany), were loaded into a planetary ball mill (PM 100, Retsch, Germany) with the recommended ball charge and filling level of the jar. In this study, the ground materials were further ground for 3 h at a speed of 400 rpm using a planetary ball mill to obtain a fine powder for slurry preparation. Then, the desired mixture and alumina balls (500 g) of 5 mm diameter were loaded into the jar of the slurry mixer and mixed for 30 min to obtain a homogenous slurry. The dipping was performed manually in a graduated cylinder (100 mL), and the dipping time was approximately 10 s. Table 2 lists the suggested coating slurries prepared to determine the optimal slurries that increase the separation rate when deposited on the inner surface of the substrates.

The main material used in preparing slurry mixtures was white clay, where the waste glass was used as an additive to reduce the pore size and form a sticky layer on the substrates when they melted during the sintering step (1200 °C). The initial amount of waste glass was 5 %; in the following two experiments, 10 and 20 % were added to each mixture. In addition, Arabic gum content was fixed at 1 % to help the coating layer deposit on the substrate surface, as it can work as an emulsifier, stabiliser, and suspending agent [15].

2.3. Characterisation techniques

The chemical compositions of the raw materials and ceramic membranes were determined using X-ray fluorescence (XRF) (JSX-3100RII Element Analyzer JEOL, Japan), whereas X-ray diffraction (XRD) (MiniFlex 600, Rigaku, Japan) with nickel-filtered Cu-Kα radiation (α = 1.5406 Å) at a scanning speed of 2° per minute in the diffraction range of 0° to 100°, was used to characterise the crystalline phases of the materials and membranes. The International Centre for Diffraction Data (ICDD), using the powder diffraction file PDF-2, was used as a reference database.

Table 2
Three different slurries were prepared to determine the optimum composition.

Material	Slurry CO-1	Slurry CO-2	Slurry CO-3
	(%)	(%)	(%)
White clay	94	89	79
Waste glass	5	10	20
Arabic gum	1	1	1
Distilled water	≈2 times the total weight of the batch	≈2 times the total weight of the batch	≈2 times the total weight of the batch

Fourier transform infrared (FTIR) spectroscopy (Agilent Cary 630 FTIR, USA), in the scanning range of 4000–600 cm^{-1} with a resolution of 4 cm^{-1}, was used to identify the functional groups of the materials and ceramic membranes, whereas the particle size distribution of the raw material powder was obtained using a laser diffraction particle size analyser (SALD-2300, Shimadzu, Japan). ASTA 8000 (PerkinElmer, Netherlands) was used for thermogravimetric analysis (TGA). The collected data provide information about the decomposition of organic materials and suggests the sintering temperature that can be subsequently applied to the fabricated substrates. A PoreMaster 33 mercury porosimeter (Quantachrome) was used to measure the pore size distribution, and substrate porosity was evaluated according to the ASTM C373-88 method [16].

The mechanical properties of the samples were measured using a Shimadzu-Universal testing machine (AGS-X, USA) with a capacity of 5 kN, total grip distance of 700 mm, crosshead speed of 0.5 mm/min, potential of 200 V, and frequency of 60 Hz. Three different membrane samples were prepared, and Equation (1) [17] was used to calculate the mechanical strength of the tubular ceramic membranes:

$$\sigma = \frac{8FLd_{outer}}{\pi\left(d_{outer}^4 - d_{inner}^4\right)} \quad (1)$$

where σ is the mechanical strength of the ceramic membrane (MPa), F is the applied load (N), L is the distance between the supports (mm), d_{outer} and d_{inner} are the outer and inner diameters of the ceramic membrane (mm), respectively. The tests were performed in triplicates.

Scanning electron microscopy (SEM; JSM-IT700HR, JOEL, Japan) was used to observe the membrane morphology.

The chemical corrosion resistance of the ceramic substrates was evaluated based on the mass loss after being subjected to acidic HCl (pH = 1.5) and alkaline NaOH solutions (pH = 13.0) at room temperature for 7 d.

2.4. Filtration test

The flux through the substrate or membrane was evaluated using an XLab 5 benchtop pilot unit (Pall Corporation, USA) (Fig. 2), which uses a crossflow filtration system. Turbidity was measured using a turbidimeter (HI 98703, HANNA, Romania). Before the experiment, three substrate samples were immersed in deionised water overnight to reduce the time required to reach a stable flux [18]. The inner surface area of the tubular substrates and membranes was calculated using the following equation to determine permeability:

$$A_{inner} = 2\pi r_2 h \quad (2)$$

where A_{inner} is the internal surface area of the tube (m^2), r_2 *is* the inner radius (m), and h is the tube height (m).

The overall dimensions for the membranes are: 6 mm I.D., 16 mm O.D. and 75 mm in length, and the permeate area for each tubular membrane tube is 1.41×10^{-3} m^2.

The permeated water was collected every 30 min in a clean water beaker and weighed using a balance to calculate the water permeate flux. The tests were performed in triplicates.

The permeability test is crucial for determining the permeate flow rate and quality in the case of contaminated feedwater. The water permeation flux can be calculated using the following equation (Darcy's law) [19].

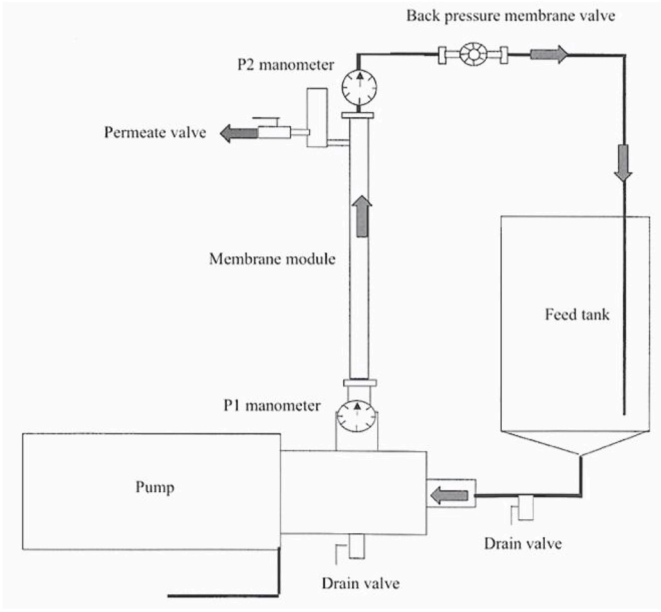

Fig. 2. Scheme of the XLab 5 benchtop pilot unit (Pall Corporation, USA).

$$J = \frac{V}{A\,t} \tag{3}$$

where J is the flux (L/m^2·h), V is the permeate volume of the collected water (L), A is the surface area of the fabricated membrane (m^2), and t is the time (h).

The permeability L_P (L/h·m^2·bar) was calculated using the following equation [19]:

$$L_P = \frac{J}{\Delta P} \tag{4}$$

where J is the flux in L/m^2·h, and ΔP is the transmembrane pressure in bar.

To calculate the transmembrane pressure in the crossflow filtration, we used the following equation [20]:

$$\mathrm{TMP} = \frac{P_F + P_C}{2} - P_P \tag{5}$$

where TMP is the transmembrane pressure (bar), P_F is the feed pressure (bar), P_C is the concentration pressure (bar), and P_P is the permeate pressure (bar).

The rejection ratio (R) was defined as the percentage of contaminants removed from the feed stream by the membrane. It was calculated using Equation (6) [19]:

$$R = \frac{C_{feed} - C_{permeate}}{C_{feed}} \times 100 \tag{6}$$

where R is the contaminant removal rate (%), C_{feed} is the feed contaminant concentration (e.g., NTU), and $C_{permeate}$ is the permeate contaminant concentration (e.g., NTU).

Table 3
Chemical composition (wt.%) of white clay, measured using XRF.

	Oxides	SiO_2	Al_2O_3	Fe_2O_3	K_2O	CaO
White clay	Wt. %	88.17	4.7	3.18	0.44	0.29

3. Results and discussion

3.1. Characterization of raw materials

Chemical composition, particle size distribution, and thermal studies were conducted to comprehend and investigate the material characteristics and make adjustments to certain properties in alignment with the objective of this study: the development of cost-effective ceramic membranes with suitable attributes for water treatment applications. To identify the chemical composition of each material, XRF was used to determine the weight percentages of metal oxides present in each material. XRD analyses were performed on each natural material powder before and after sintering to identify the crystalline phases present in each material. FTIR spectroscopy was employed to identify the functional groups of each material and to detect any changes in the chemical structure after sintering.

3.1.1. White clay

The chemical composition of white clay in terms of weight percentage (wt.%) of the oxides is given in Table 3. The white clay consists of SiO_2 (88.17 wt%), Al_2O_3 (4.7 wt%), and Fe_2O_3 (3.18 wt%), along with trace amounts of other metal oxides.

Using XRD, quartz (reference code:00-046-1045), silica (reference code:00-033-1161), alumina (reference code:00-010-0173), and hematite (reference code:00-024-0072) were identified as the major crystalline phases of the white clay samples before sintering. After sintering at 1000 and 1200 °C, there was a transition in the crystalline phase; specifically, there were obvious peaks which represented the formation of the cristobalite phase when sintered at 1200 °C with a holding time of 1 h [17]. Fig. 3 shows the diffraction patterns before and after sintering at 1000 and 1200 °C with a soaking time of 1 h.

Fig. 4 shows the IR spectra of the white clay specimens as raw materials and sintered at 1000 and 1200 °C. The bands at 3617–3750 cm^{-1} were due to the stretching vibration of the O–H bond and the HO–H vibration of adsorbed water molecules in the raw white clay specimen [21]. These bands were absent when the white clay specimens were sintered. The bands at approximately 694, 778, 797, and 1082 cm^{-1} of raw white clay were assigned to the presence of Si–O symmetrical stretching vibrations [22]. Additionally, the sharp band at approximately 912 cm^{-1} and the weak shoulder at 940 cm^{-1} were due to Al (VI)–OH vibrations [23].

3.1.2. Silica flour

The silica flour (silica sand powder) composition was dominated by SiO_2 (99.8 %), followed by a small weight percentage of Fe_2O_3 (0.16 %), as shown in Table 4.

Using XRD, quartz (reference code:00-046-1045), silica (reference code:00-033-1161), and hematite (reference code:00-024-0072) were identified as the major crystalline phases in the untreated silica flour sample. Fig. 5 shows no change in the diffraction patterns of the silica flour samples after sintering at 1200 °C with a holding time of 1 h.

Fig. 6 shows the IR spectra of the silica flour specimens as raw material and sintered at 1200 °C. In both spectra, the peaks at 691, 773, 795, 1051, and 1161 cm^{-1} were assigned to the presence of Si–O

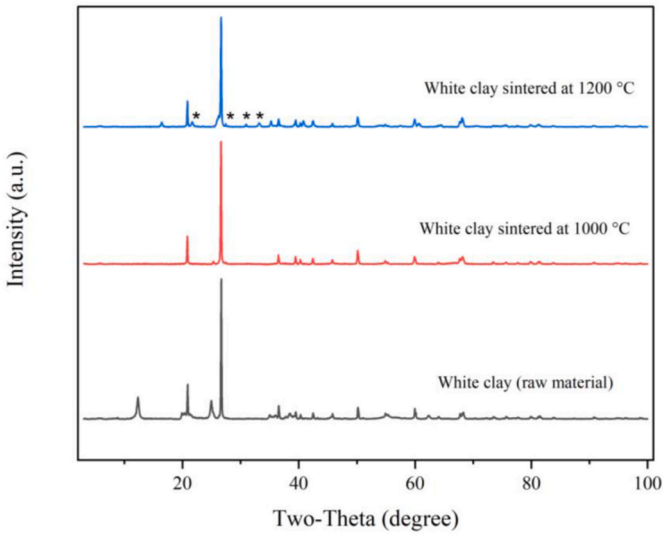

Fig. 3. X-ray diffraction of white clay before and after sintering at 1000, and 1200 °C; (*) represents the peaks that confirm the formation of the cristobalite phase at 1200 °C.

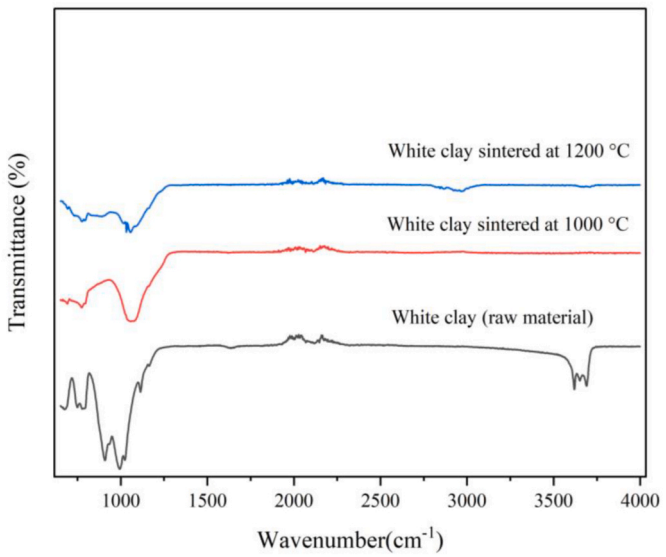

Fig. 4. FTIR spectra of white clay sintered at different temperatures.

Table 4
Chemical composition (wt. %) of silica flour using X-Ray fluorescence (XRF).

	Oxides	SiO_2	Fe_2O_3
Silica flour	Wt. %	99.83	0.16

symmetrical stretching vibrations [22], with no change in their wavenumber position. The two peaks at 1420 and 1494 cm^{-1} may be attributed to the carbonate group in calcite or organic matter [24]. The small band at 1641 cm^1 is due to the bending H–OH bond of adsorbed water molecules of untreated silica flour [21].

3.1.3. Marble powder

To determine the percentage of calcium carbonate in marble powder, an acid-base titration analysis was performed, showing that marble powder contained approximately 96 % of calcium carbonate.

The XRD spectrum of the raw marble powder was identical to that of

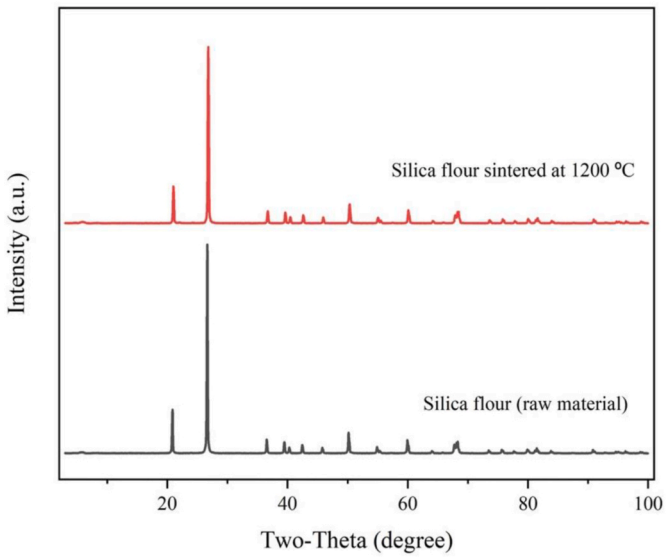

Fig. 5. X-ray diffraction of silica flour before and after sintering at 1200 °C.

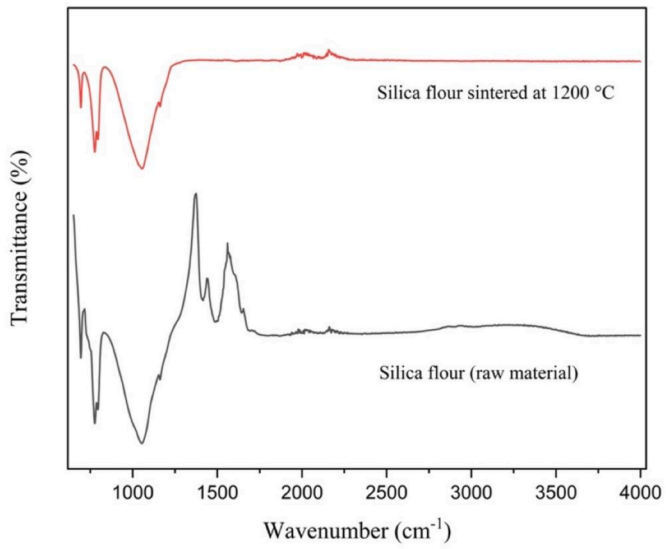

Fig. 6. FTIR spectra of raw silica flour and silica flour sintered at 1200 °C.

calcite ($CaCO_3$) (reference code:00-005-0586). When the marble powder was sintered at 1200 °C, $CaCO_3$ decomposed into CaO and CO_2. However, CaO easily reacts with moisture to produce $Ca(OH)_2$. Fig. 7 shows the marble powder diffraction patterns before and after sintering at 1200 °C for a holding time of 1 h. In addition, peaks at $2\theta = 28.6°$, 34.1°, 47.1°, and 50.8° were observed, indicating $Ca(OH)_2$ formation [25].

Fig. 8 shows the IR spectra of the marble powder specimens as raw material and sintered at 1200 °C. The peaks at 713, 877, 1431, 1799, and 2517 cm^{-1} were assigned to carbonate in the raw marble powder spectrum [26]. The absence of the peak at 713 cm^{-1} indicates that $CaCO_3$ was converted into CaO after sintering [26]. The peak at approximately 3600 cm^{-1} was attributed to the O–H stretching vibration of adsorbed water [26].

3.2. Optimizing substrates selection

To determine the optimal mixture of substrates A and B, the objectives for fabricated substrate A were to achieve the maximum flux and

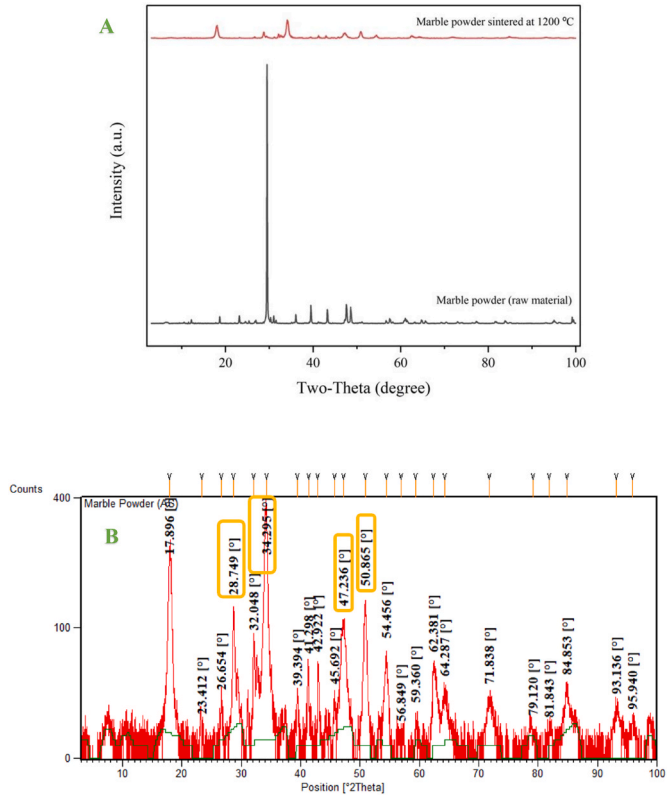

Fig. 7. (A) X-ray diffraction of marble powder before and after sintering at 1200 °C. (B) Peaks that represent $Ca(OH)_2$ formation are highlighted.

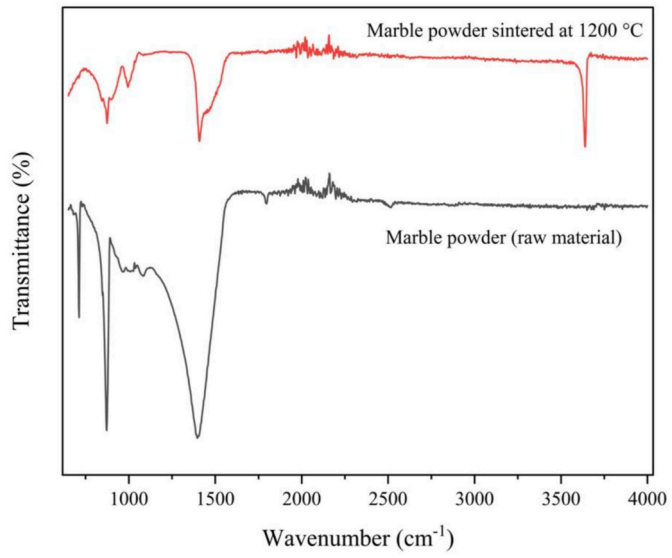

Fig. 8. FTIR spectra of raw marble powder and marble powder sintered at 1200 °C.

bending strength. Meanwhile, for fabricated substrate B, the goals were to attain the maximum flux, bending strength, and minimum mass loss, following the corrosion test in acidic media. After fabrication of all batches suggested by the JMP software (Table 1), we measured the flux and bending strength for the substrates, and for the batches of substrate B, we also determined the percentages of mass loss after the corrosion test in acidic media. After gathering these results (Table 5), it became possible to run the model and establish the optimal recipes for fabricating substrate A (white clay: 62.7 %, silica flour: 32.3 %, and Arabic gum: 5 %) and substrate B (white clay: 63 %, silica flour: 26.8 %, and marble powder: 10.2 %). Further details can be seen in Texts 1.S and 2.S (Supplementary Information).

Table 5
Flux, bending strength results for both substrates A and B and corrosion test (acidic media) for substrate B (△P = 0.75 bar; feed water is distilled water for flux evaluation).

Number	Substrate A		Substrate B		
	Flux (L/hm^2)	bending strength (MPa)	Flux (L/hm^2)	bending strength (MPa)	Percentages of mass loss (Wt.%), pH = 1.5
1	50	31	116	32	0.68
2	101	14	102	39	2.7
3	63	28	75	37	0.7
4	158	11	190	36	2.67
5	186	10			
6	170	9			
7	95	8			
8	142	10			
9	49	22			

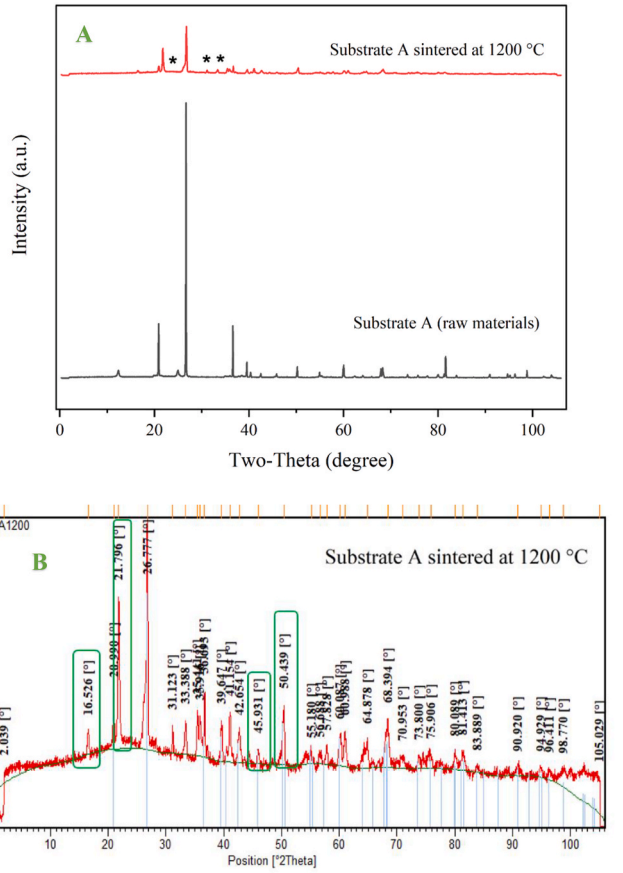

Fig. 9. (A) X-ray diffraction of substrate A before and after sintering at 1200 °C (B). Peaks that represent mullite ($Al_6Si_2O_{13}$) are highlighted [27].

3.3. Substrates characterizations

Substrates A and B were subjected to XRD analysis before and after sintering to investigate the potential reactions among the constituting natural materials. In addition, FTIR spectroscopy was conducted to identify the functional groups of each material and detect any changes in the chemical structure after sintering.

Peaks representing the cristobalite phase were observed when the

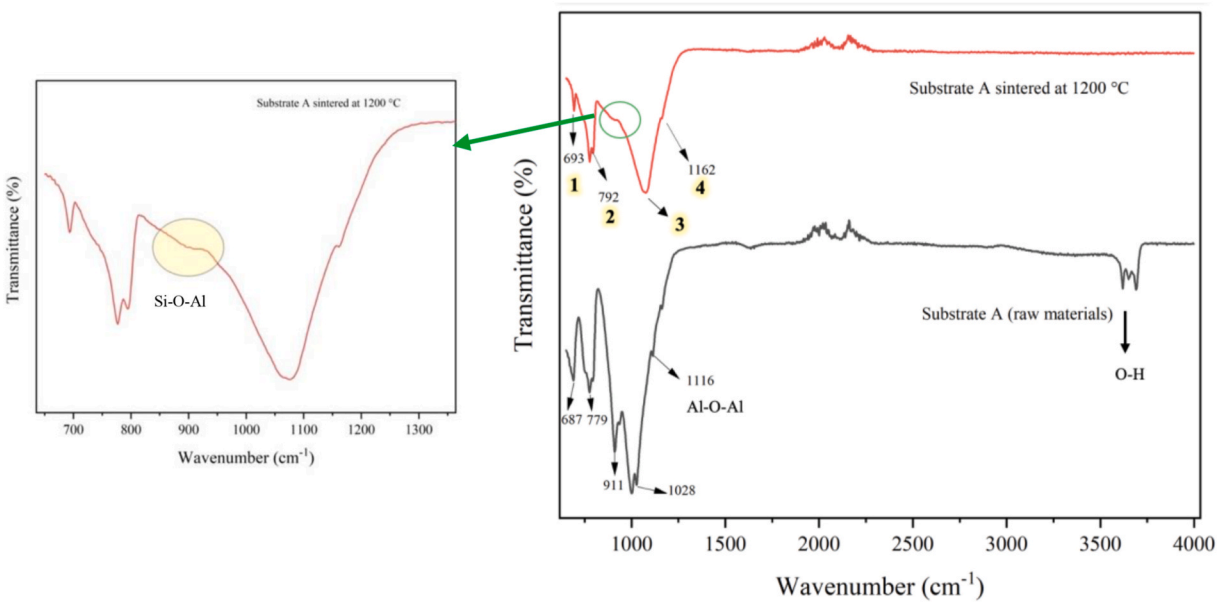

Fig. 10. FTIR spectra of substrate A before and after sintering at 1200 °C.

mixture of substrate A was sintered at 1200 °C, as shown in Fig. 9. In addition, mullite ($Al_6Si_2O_{13}$) was formed as a result of the reaction between silica and alumina when the mixture of substrate A was sintered at 1200 °C.

Fig. 10 shows the IR spectra of substrate A specimens as the raw material and sintered at 1200 °C. For the spectrum of substrate A before sintering, the sharp band at approximately 912 cm^{-1} and the weak shoulder at 940 cm^{-1} were due to the Al(VI)–OH vibrations [28], and the peak at approximately 3600 cm^{-1} was attributed to the O–H stretching vibration of the adsorbed water [26]. For the spectrum of substrate A after sintering, the peaks at 693, 792, 1082, and 1162 cm^{-1} were assigned to silica in the substrate A spectrum [22]. The broad peak at 902 cm^{-1} is attributed to the Si–O–Al bond, which is a result of the reaction between SiO_2 and Al_2O_3 [28].

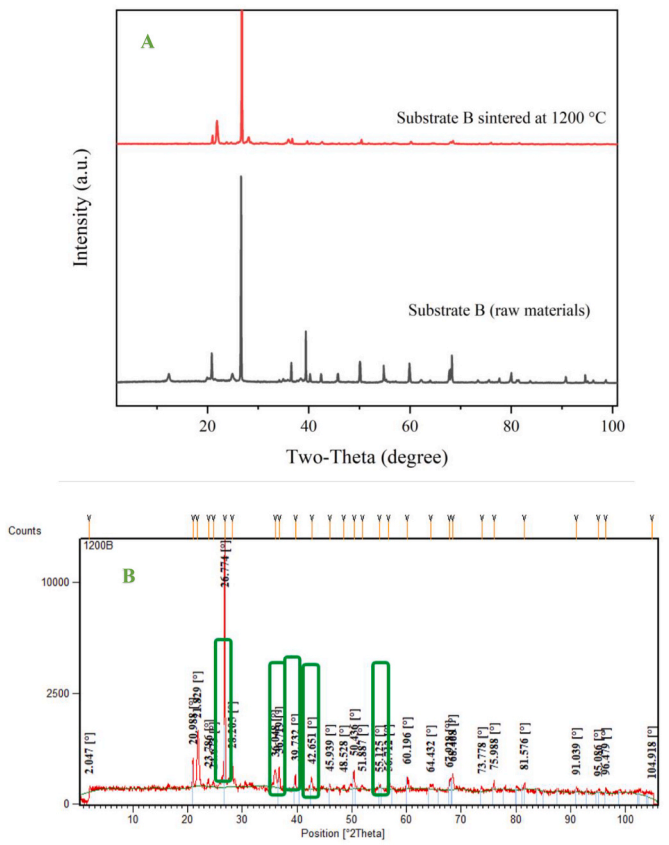

Fig. 11. (A) X-ray diffraction of substrate B before and after sintering at 1200 °C (B). Peaks that represent wollastonite ($CaSiO_3$) (JCPDS 74–0874) are highlighted [27].

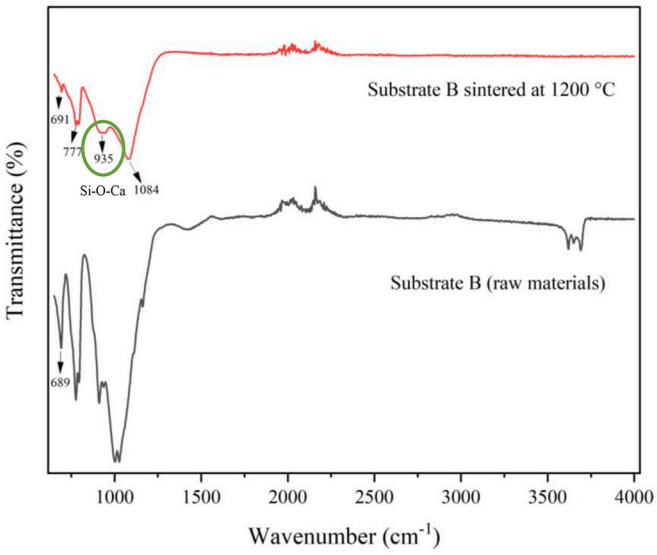

Fig. 12. FTIR spectra of substrate B before and after sintering at 1200 °C.

The XRD spectrum of substrate B was identical to that of wollastonite ($CaSiO_3$) (JCPDS 74–0874) when sintered at 1200 °C with a holding time of 1 h. The formation of wollastonite was a result of the reaction between SiO_2 and CaO (after the thermal decomposition of $CaCO_3$) present in the mixture of substrate B. Fig. 11 shows the substrate B diffraction patterns before and after the sintering step.

Fig. 12 shows the IR spectra of substrate B specimens as the raw material and sintered at 1200 °C. In the spectrum of substrate B after sintering, the peaks at 691, 777, and 1084 cm^{-1} were assigned to silica in the substrate B spectrum [22], while the peak at 935 cm^{-1} was

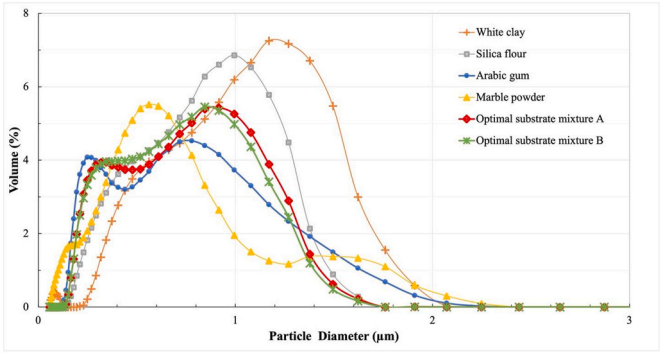

Fig. 13. Particle size distribution of raw materials and the optimal substrates mixtures of A and B.

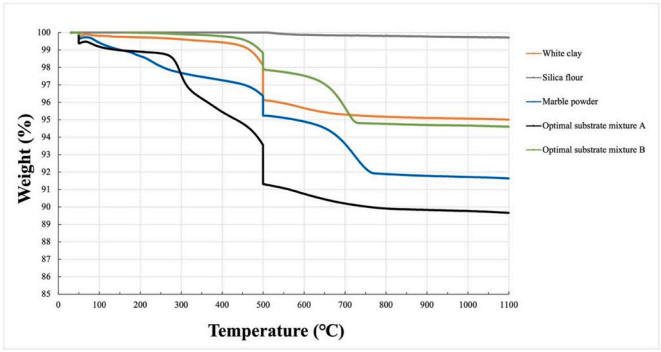

Fig. 14. TGA analysis of raw white clay, silica flour, marble powder, and optimal substrate mixtures A and B.

attributed to the Si–O–Ca bond which indicates calcium wollastonite formation [29].

The particle size distribution of raw materials is important, because it directly improves the stability of the substrate and prevents the formation of holes in its structure. In addition, Reed [13] reported that flow resistance decreased as the particle size decreased. The average particle size distributions of the three raw materials used to develop substrate A were 1.315 μm for white clay, 1.068 μm for silica flour, and 0.828 μm for the pore-forming agent (Arabic gum). For substrate B fabrication, marble powder, which had an average particle size of 0.738 μm, was used as the pore-forming agent instead of Arabic gum. The mean particle sizes of substrates A and B were 0.885 and 0.738 μm, respectively.

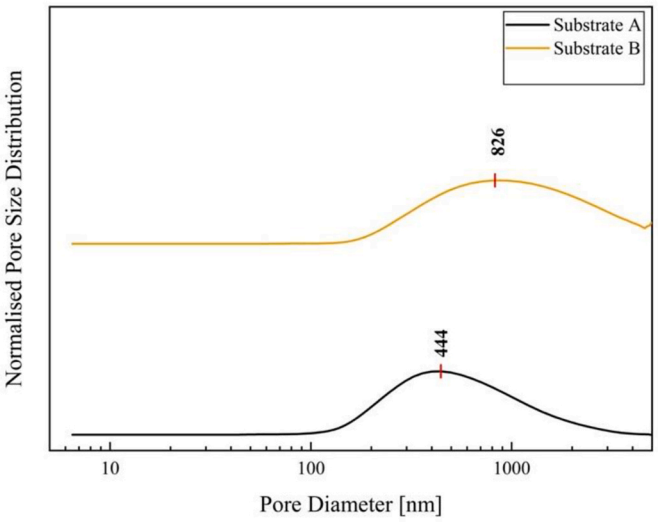

Fig. 16. Pore size distributions of substrate A and substrate B, as measured by mercury porosimetry.

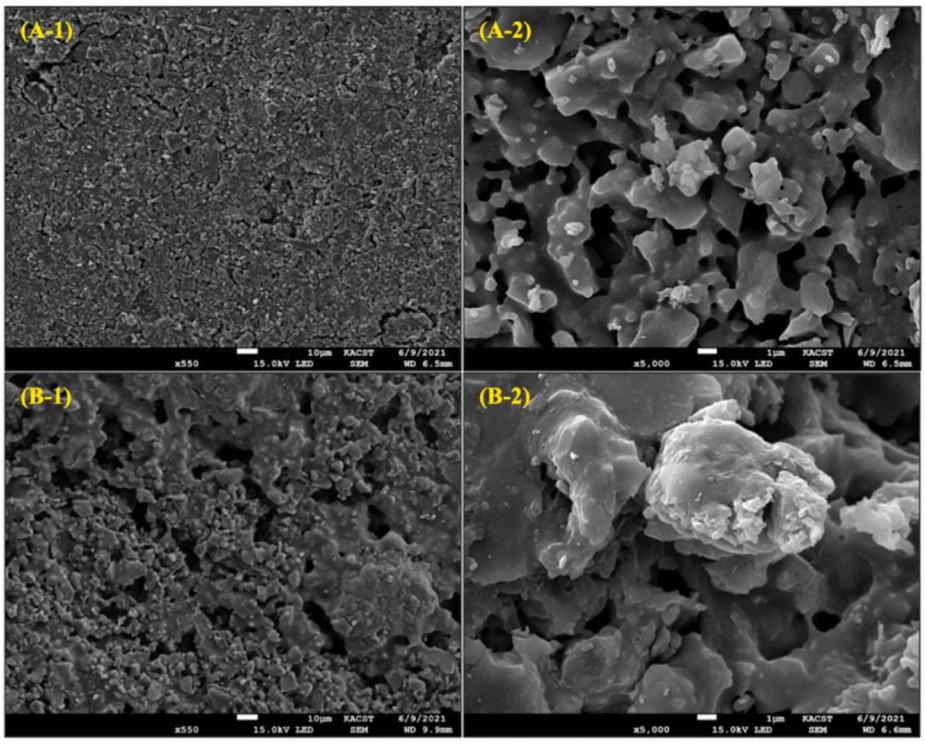

Fig. 15. SEM images of the surface of substrate A (A-1 and A-2), and substrate B (B-1 and B-2), A-1 and B-1 images at 550 × magnification, whereas A-2 and B-2 images at 5000 × magnification.

Fig. 13 shows the particle size distribution of the raw materials and optimal substrate mixtures of A and B using a laser diffraction particle size analyser (SALD-2300, Shimadzu, Japan).

The effect of temperature on the raw materials and their mixtures was investigated using TGA. Fig. 14 shows the weight loss of the raw materials and their mixtures (substrate mixtures A and B). There was a slight decrease of approximately 4 % in the weight of white clay at 500 °C, which might have occurred because of organic content decomposition, whereas almost no change was observed in the silica flour weight, possibly because it had a relatively high purity. Above 800 °C, there were no appreciable changes in weights of optimal substrate mixtures A and B.

The SEM images of the fabricated ceramic substrates A and B show a rough surface morphology, with no apparent deep cracks or defects on either substrate (Fig. 15).

The pore size distributions of the fabricated substrates A and B were centred at 444 and 826 nm, respectively, as measured by mercury porosimetry (Fig. 16).

3.4. Characterization of optimized membranes with a coating layer on the substrates

In this study, waste glass was employed in three coating slurries to generate an adhesive layer on the substrates during the sintering phase. For example, Fig. 17 shows an image of substrate A with coating layer CO-1 and an SEM image of the cross-section of the coating layer with a thickness of approximately 21 μm at 55 × magnification. In addition, pore size reduction was influenced by the amount of waste glass added. The pore size distributions of CO-1, CO-2, and CO-3 slurries containing 5 %, 10 %, and 20 % waste glass, respectively, are presented in Fig. 18, showing peak values of 348, 109, and 14 nm, respectively.

In addition, using the same material for both the membrane layer and the support yields a uniform membrane layer that adheres strongly to the support, while also preventing the development of surface cracks during thermal treatment. As previously mentioned, the dip-coating technique was used for membrane layer deposition. In Fig. 17 (a) and

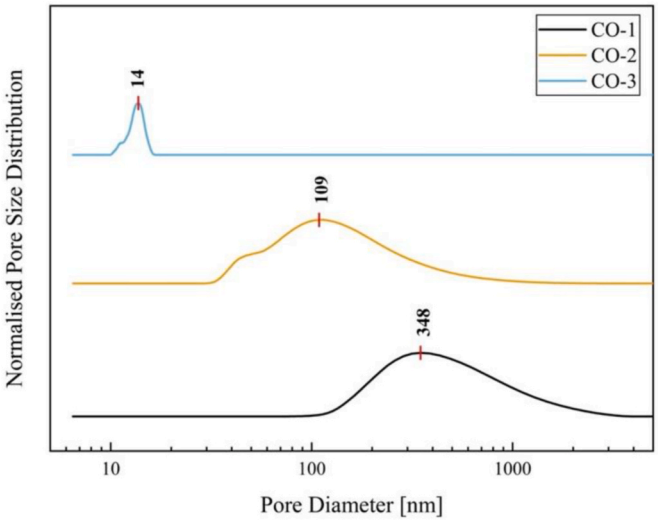

Fig. 18. Pore size distribution of coating layer CO-1, CO-2, and CO-3 were measured by mercury porosimetry.

17(b), the sintered ceramic membrane is examined using top-view and cross-sectional SEM images, which reveal its uniformity, smoothness, and homogeneity without any defects. The observed low agglomeration can be attributed to increase in particle size and the enlargement grain boundaries that occur as a result of sintering. The cross-sectional image enabled the estimation of the membrane layer thickness, revealing it to be 21 μm, and confirming the strong adherence of the membrane to the support. Mouiya et al. [19] observed a similar behaviour.

After sintering at 1200 °C, there were obvious peaks, which represented borosilicate glass [30], quartz and silica. Fig. 19 shows the diffraction pattern of the coating layer CO-2 after sintering.

Fig. 20 shows the IR spectra of the coating layer CO-2 specimen, which sintered at 1200 °C. In the spectrum, the band at 669 cm^{-1} is assigned to BO_3. [30], while the peaks at 694, 778, and 797 cm^{-1} were

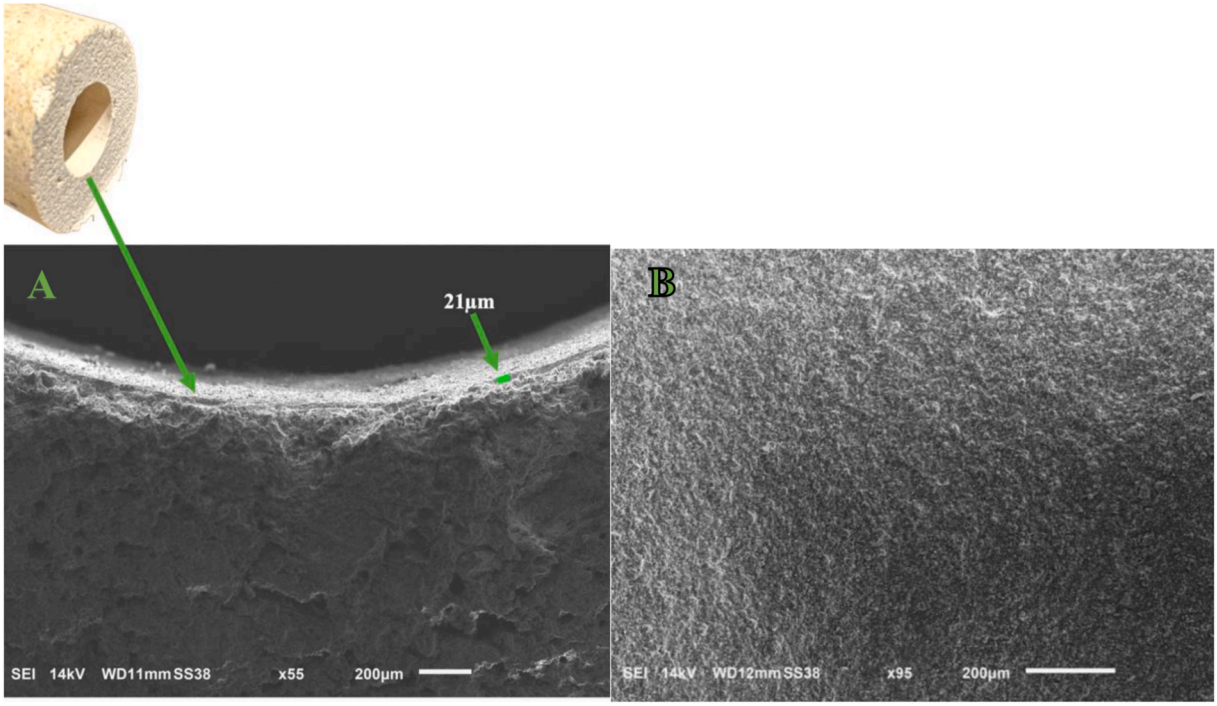

Fig. 17. (A) An image of substrate A with coating layer CO-1 and an SEM image at 55 × magnification of the cross-section of the coating layer with a thickness of approximately 21 μm. (B) SEM image of the coating layer (top view) at 95 × magnification.

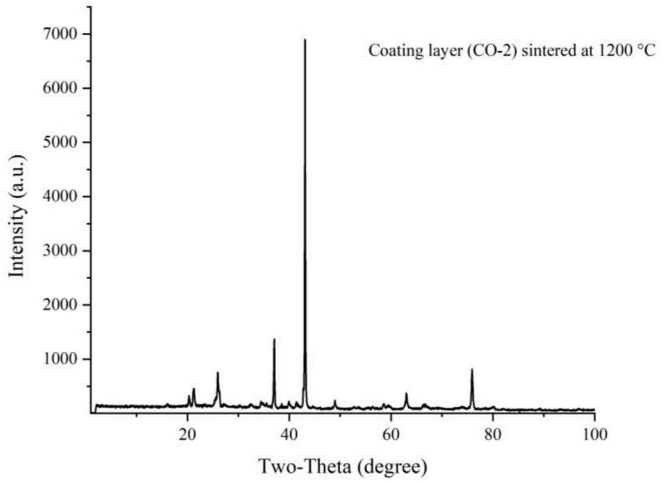

Fig. 19. X-ray diffraction of coating layer after sintering at 1200 °C.

assigned to silica [22].

3.5. Evaluation of fabricated membranes performance

3.5.1. Evaluation of the optimal substrates

An important measure of the performance of a ceramic substrate is the flux, which is typically assessed using a crossflow filtration system. Figs. 21 and 22 show the flux stability over time for substrates A and B, respectively, using deionised water as the permeate. Table 6 provides a comprehensive summary of both substrates, outlining key metrics, such as flux, bending strength, corrosion test results, porosity, bulk density, and apparent specific gravity.

According to the data in Table 6, substrate B demonstrated a higher flux of 116 L/m^{2}h, compared to substrate A's flux of 77 L/m^{2}h. This was probably due to its higher porosity of 34 %, compared to substrate A's porosity of 29 % [31]. In a study conducted by Bouzerara et al. [32], a higher flux was also attributed to the increased porosity of membranes with higher porosity, enabling a greater flow of water through the membrane. Overall, these studies support the notion that increased porosity in ceramic membranes can result in higher flux rates. However, this requires further investigation as tortuosity and connectivity of the pores may also affect the flux [33].

Moreover, sintering at 1200 °C increased the bending strength for both substrates A and B. Sintering below this temperature would result in lower bending strength and an unstable structure. For example, an attempt was made to sinter the fabricated membranes at 1000 °C. However, there was a decline in the flux over time, despite the use of pure water in this experiment. The XRD results of white clay displayed a clear transition in the crystalline phase upon sintered at 1200 °C. For silica flour, no transition in the crystalline phase occurred even at 1200 °C. However, the XRD and FT-IR results showed the formation of different crystalline phases and new bonds (Figs. 9–12) when a mixture of these materials was used and sintered at 1200 °C. Therefore, it is not possible to obtain a stable structure that can resist the applied pressure without collapsing when sintering is performed below 1200 °C. For example, Ivanets et al. [34] reported a decline in the flux over time when using the drinking water of Minsk city as feed water. Quartz sand was

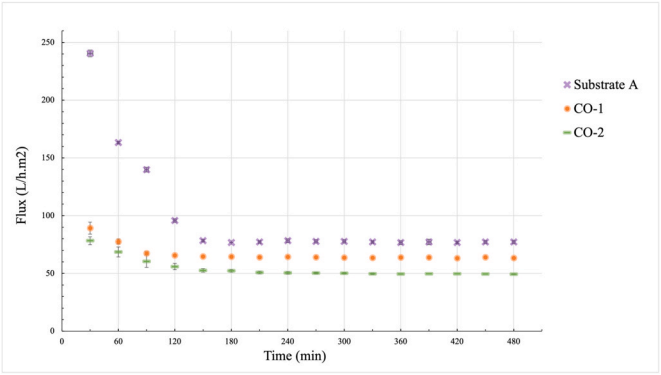

Fig. 21. Permeate flux as a function of filtration time of coated substrate A; △P = 0.75 bar, feed: distilled water.

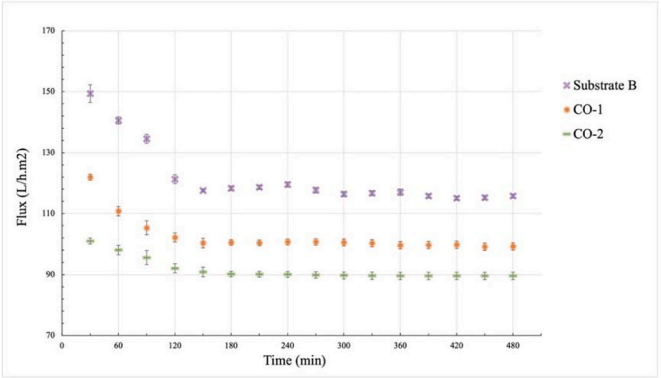

Fig. 22. Permeate flux as a function of filtration time of coated substrate B; △P = 0.75 bar, feed: distilled water.

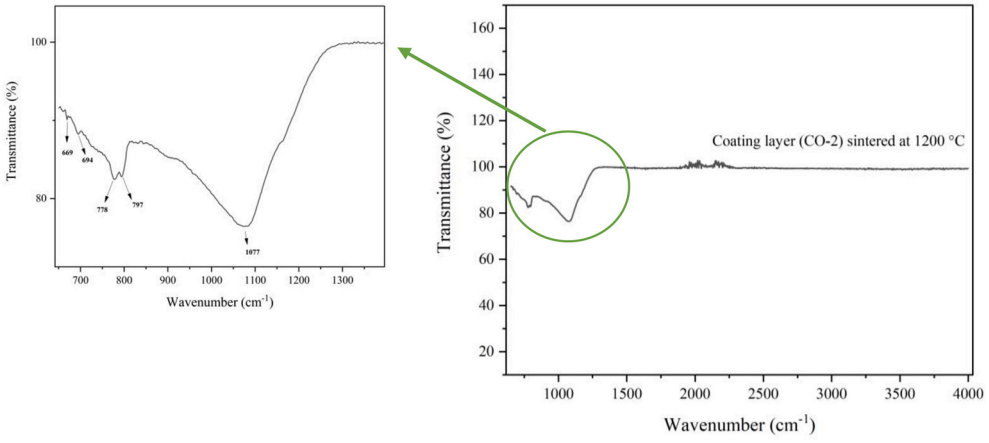

Fig. 20. FTIR spectrum of the coating layer CO-2 after sintering at 1200 °C.

Table 6
Some properties of substrates A and B.

Number	Flux[a] (L/hm^2)	Bending strength (MPa)	Percentages of mass loss (Wt.%), pH = 1.5	Percentages of mass loss (Wt.%), pH = 13	Porosity (%)	Water absorption (%)	Bulk density (g/cm^3)	Apparent specific gravity
Substrate A	77	26.4	0.0	0.0	28.7	17.8	1.64	2.25
Substrate B	116	38.9	1.42	0.0	33.86	20.7	1.63	2.47

[a] Average flux was measured after 2 h of filtration.

used in the fabrication of their ceramic membranes, which were sintered at 600 °C.

Studies have shown a positive correlation between bending strength and temperature sintering of ceramics. For example, Wan et al. [35] investigated the effects of various sintering parameters on the mechanical properties of fused silica ceramics. According to their findings, elevating the sintering temperature resulted in an enhancement of both the bending strength and the stability of the ceramics.

Substrate A, which contains Arabic gum, was heated from 100 °C to 500 °C at a rate of 5 °C per min. Meanwhile, substrate B, which consists of marble powder with a calcium carbonate content of over 96 %, was heated from 100 °C to 800 °C at the same rate. According to the TGA results presented in Fig. 15, calcium carbonate decomposition into CaO and CO_2 at 800 °C required a higher temperature for substrate B. XRD analysis revealed that when substrate A was sintered at 1200 °C, it produced mullite ($Al_6Si_2O_{13}$) owing to the reaction between alumina and silica, while substrate B formed wollastonite ($CaSiO_3$), indicating a difference in the structure of the two substrates. The difference in the bending strength between substrate A (26.4 MPa) and substrate B (38.9 MPa), as shown in Table 6, can be attributed to the mechanical properties of wollastonite, which enhanced substrate strength. Overall, the XRD analysis highlights that the variance in substrate structure accounts for the differences in bending strength.

Additionally, Table 6 displays the optimal substrates that were subjected to rigorous testing in highly acidic and basic media to assess their chemical resistance. Mass loss was determined after exposure to an HCl solution with a pH of 1.5 and a NaOH solution with a pH of 13 at room temperature for seven days. The results show that the mass loss ranged from 0 wt% to 1.42 wt% in acidic solution and 0 wt% in basic solution. These findings align with those of clay-based ceramic membranes as reported in the literature, even though earlier research has shown that the produced membranes have low resistance to acid corrosion [19]. Moreover, the stability of both substrates, A and B, was tested at pH = 7, and the results demonstrated no mass loss for either substrate.

3.5.2. Evaluation of the optimal membranes with a coating layer on substrates

Figs. 21 and 22 illustrate the evolution of the membrane water flux using deionised water as the permeate. The results indicate a decline in the flux following top-layer deposition. This outcome was anticipated because the top layer is expected to have a smaller pore size. Ali et al. [36] reported similar results when assessing the water flux of ceramic membranes fabricated from natural kaolino-illitic clay supports and using deionised water as the permeate. They observed a reduction in flux after depositing the top layer, which was expected due to the typically smaller pore sizes found in the top layer. Membranes with coating layer CO-3 exhibited a low flux below 5 L/m^{2}h, as a result, they were excluded from the remaining flux and separation experiments.

A commercial ultrafiltration ceramic membrane with a 300 kg/mol cut-off, featuring a substrate composed of TiO_2 and an active layer made of ZrO_2, was purchased from TAMI Industries, France. The purpose of using this commercial ceramic membrane was to compare its performance, especially regarding membrane water flux, with the results obtained in this study when deionised water was used as the permeate. The findings revealed a flux of approximately 100 L/m^{2}h for the commercial membrane. Notably, one of the membranes fabricated in this study, specifically substrate B with a coating layer (CO-1), exhibited an equivalent flux value. Table 7 presents some previous studies on the fabrication of ceramic membranes, providing information on the materials employed, average pore size, and permeability as measured using

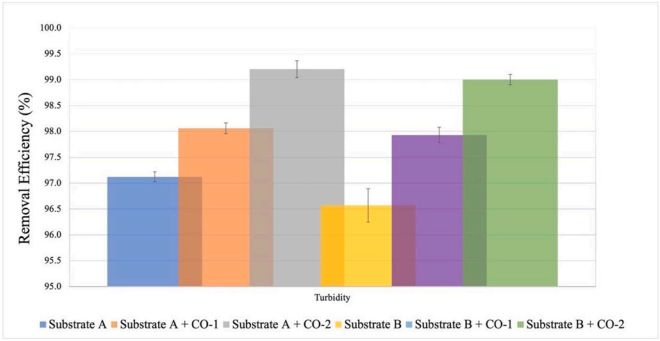

Fig. 23. Turbidity removal efficiency of fabricated membranes; △P = 0.75 bar; backwash every 2 h; feed water, tap water, and bentonite clay; average particle size of bentonite clay, 1.1 μm; turbidity, 13 ± 0.2 NTU.

Table 7
An overview of properties of ceramic membranes fabricated by low-cost materials.

Ref.	Filtration mode	Main material	Average pore size (μm)	Permeability[a] (L/h m^{2}bar)
[37]	Microfiltration	Alumina, and starch	1–5	405.9
[38]	Microfiltration	Fly ash - clay mixture	0.64	153
[12]	Microfiltration	Kaolin, quartz, calcium carbonate, sodium carbonate, boric acid, and sodium metasilicate	0.3–0.6	83.6
This work	Microfiltration	Substrate A: white clay (62.7 %), silica flour (32.3 %), and Arabic gum (5 %). Substrate B: white clay (63 %), silica flour (26.8 %), and marble powder (10.2). Coating layer: white clay, waste glass and Arabic gum (different percentage).	Substrate A: 0.44 Substrate B: 0.83 (C0-1): 0.35 (C0-2): 0.11	Substrate A: 103 Substrate A with coating layer 1 (C0-1): 85 Substrate A with coating layer 2 (C0-2): 67 Substrate B: 156 Substrate B with coating layer 1 (C0-1): 133 Substrate B with coating layer 2 (C0-2): 120

[a] Permeability was measured using pure water.

pure water.

Regarding separation performance, the fabricated membranes demonstrated effective turbidity separation of synthetic feed water composed of tap water and bentonite clay, with an average particle size of 1.1 μm and turbidity of 13 ± 0.2 NTU, as shown in Fig. 23. Further details can be found in the supporting information (Fig. 1.S and 2.S). Notably, the membrane composed of substrate A with a coating layer of CO-2 exhibited the highest capacity for bentonite clay particles, achieving an impressive rejection rate of approximately 99.2 %. This exceptional performance can be attributed to the fact that both the substrate and CO-2 coating layer had the smallest pore size among all the fabricated membranes. However, the flux of this membrane was relatively low, approximately 42 L/m^2 h, in comparison to other fabricated membranes in this study.

For future studies, further research on separation will be undertaken, with a specific focus on applications such as employing these membranes to remove fouling-causing substances during the pre-treatment stage of the reverse osmosis system.

4. Membrane cost

Ceramic membrane costs are estimated to be between 500 and 3000 USD/m^2, typically [9]. Using low-cost materials that do not require high sintering temperatures can minimise the cost of ceramic membranes to make them affordable. However, it is important to note that reliability, stability, and robustness are significant features of any new, low-cost ceramic membrane. Based on the costs of the raw materials (Table 8) and energy consumption (Table 9) used for fabricating the ceramic membranes in this study, the cost of ceramic membranes A and B was estimated to be approximately 51 and 47 USD/m^2, respectively.

These estimates indicate the potential for producing ceramic membranes at a significantly reduced cost, making them more affordable and accessible for a wide range of industrial applications. The cost of ceramic membranes significantly affects their widespread adoption, particularly for large-scale applications. By lowering production cost, a broader range of industries and applications can take advantage of the distinctive properties of ceramic membranes, including their high selectivity, durability, and resistance to harsh environments.

5. Conclusions

Two ceramic membranes were fabricated through an extrusion process: substrate A and substrate B. The optimal composition for each was determined to be: for substrate A, white clay (62.7 %), silica flour (32.3 %), and Arabic gum (5 %); and for substrate B, white clay (63 %), silica flour (26.8 %), and marble powder (10.2 %). The primary constituent of the coating layer was white clay, with waste glass added as an admixture at a 5 % concentration to shrink the pore size. When sintered at 1200 °C, this mixture formed a cohesive layer on the substrates. A fixed 1 % of Arabic gum was also incorporated to facilitate the adhesion of the coating to the substrate surface.

The membranes were evaluated using several techniques, including X-ray fluorescence spectrometry, X-ray diffraction, Fourier-transform infrared spectroscopy, laser diffraction particle size analysis, thermogravimetric analysis, and a universal testing machine. The surface morphology was analysed using SEM, and the resulting images of ceramic substrates A and B showed a rough appearance. Neither substrate exhibited noticeable cracks or imperfections. The resistance of the ceramic substrates to chemical corrosion was assessed by measuring the mass loss after exposure to an acidic solution of HCl (pH = 1.5) and an alkaline solution of NaOH (pH = 13.0) at room temperature for 7 d. The results showed that there was no mass loss in alkaline media. However, in the acidic media, only substrate B experienced a mass loss of 1.42 %. The flow rate of the substrates was determined using a crossflow filtration system, revealing that substrate B exhibited a higher flow rate (116 L/m^{2}h) than substrate A (77 L/m^{2}h). This difference can be

Table 8
Cost of the raw materials.

Membrane	Substrate/Coating layer	Raw materials	Percentage of raw materials (%)	Cost (USD/kg)	The total cost of raw materials that were used to fabricate 1 m^2 (USD/m^2)
Membrane A	Substrate A	White clay	62.7	1.3	12.7
		Silica flour	32.3	0.27	
		Arabic gum	5	9.3	
	Coating layer	White clay	94	1.3	
		Waste glass	5	0.13	
		Arabic gum	1	9.3	
Membrane B	Substrate B	White clay	62.7	1.3	8.5
		Silica flour	32.3	0.27	
		Marble powder	5	0.22	
	Coating layer	White clay	94	1.3	
		Waste glass	5	0.13	
		Arabic gum	1	9.3	

Table 9
Cost of the electricity consumption.

No.	Machine	Time (h)	Energy consumption (kWh per hour)	Energy consumption to fabricate 1 m^2 of ceramic membranes (kWh)	Cost based on average global electricity price (USD)
1	Fritsch disc mill	0.5	0.5	0.25	0.032
2	Roller mixer	0.3	0.25	0.075	0.001
3	High-speed mixer	0.25	1.1	0.275	0.035
4	Extruder	0.15	1.48	0.222	0.028
5	Electric furnace	15	20	300	38.1
6	Planetary ball mill	3	1.25	3.75	0.48
7	Slurry mixer	0.3	0.7	0.21	0.026
Total				305	38.7

attributed to its higher porosity (34 %) compared to that of substrate A (29 %). All membranes showed high removal efficiency, exceeding 96 % for synthetic feed water consisted of tap water and bentonite clay.

The production costs of ceramic membranes A and B were estimated to be 51 and 47 USD/m^2, respectively, making them a cost-effective choice. This means that fabricated ceramic membranes are a viable option to consider for brackish water purification at a much lower cost than commercial ceramic membranes, which can cost anywhere from 500 to 3000 USD/m^2. In conclusion, the results of this study indicate that the fabricated ceramic membranes are promising and could be considered for brackish water purification using low-cost materials that do not require high sintering temperatures. This reduces the cost of ceramic membranes to a more affordable level, making them more accessible for widespread use.

Although the study suggests that the fabricated ceramic membranes A and B are cost-effective, some limitations should be highlighted. Firstly, the study exclusively addressed the performance and cost of the membranes under laboratory conditions. Consequently, the real-world performance of these membranes, particularly in larger-scale systems or over extended periods, may deviate from the laboratory results. Furthermore, additional research is required to provide more information on the durability and lifespan of the fabricated ceramic membranes. Factors such as membrane fouling and degradation over time can impact the performance and cost-effectiveness of the membranes, and these aspects were not addressed in the study.

CRediT authorship contribution statement

Mohammed D. Alsubei: Conceptualization, Investigation, Methodology, Formal analysis, Data Curation, Writing – Original draft, Visualization, Funding acquisition. **Barry Reid:** Investigation, Visualization, Writing - review & editing. **Saad A. Aljlil:** Resources, Writing - Review & Editing. **Marc-Olivier Coppens:** Conceptualization, Methodology, Resources, Writing – review & editing, Supervision. **Luiza C. Campos:** Conceptualization, Methodology, Writing – review & editing, Supervision, Project administration, Funding acquisition.

Declaration of competing interest

The authors declare that they have no known competing financial interests or personal relationships that could have appeared to influence the work reported in this paper.

Data availability

Data will be made available on request.

Acknowledgements

The authors extend their gratitude to the King Abdul Aziz City for Science and Technology (KACST) for funding Mr Mohammed Alsubei.

Appendix A. Supplementary data

Supplementary data to this article can be found online at https://doi.org/10.1016/j.memsci.2023.122226.

References

[1] R. Chihi, I. Blidi, M. Trabelsi-Ayadi, F. Ayari, Elaboration and characterization of a low-cost porous ceramic support from natural Tunisian bentonite clay, Compt. Rendus Chem. 22 (2–3) (2019) 188–197.
[2] W.-i. Park, S. Jeong, S.-J. Im, A. Jang, High turbidity water treatment by ceramic microfiltration membrane: fouling identification and process optimization, Environ. Technol. Innovat. 17 (2020), 100578.
[3] A. Ivanets, V. Agabekov, Ceramic microfiltration membranes based on natural silica, Petrol. Chem. 57 (2) (2017) 117–126.
[4] P. Jarvis, I. Carra, M. Jafari, S.J. Judd, Ceramic vs polymeric membrane implementation for potable water treatment, Water Res. 215 (2022), 118269.
[5] K. Li, Ceramic Membranes for Separation and Reaction, John Wiley & Sons, 2007.
[6] K.A. DeFriend, M.R. Wiesner, A.R. Barron, Alumina and aluminate ultrafiltration membranes derived from alumina nanoparticles, J. Membr. Sci. 224 (1–2) (2003) 11–28.
[7] Y.H. Wang, T.F. Tian, X.Q. Liu, G.Y. Meng, Titania membrane preparation with chemical stability for very hash environments applications, J. Membr. Sci. 280 (1–2) (2006) 261–269.
[8] T. Tsuru, Inorganic porous membranes for liquid phase separation, Separ. Purif. Methods 30 (2) (2001) 191–220.
[9] S.L.S. Rani, R.V. Kumar, Insights on applications of low-cost ceramic membranes in wastewater treatment: a mini-review, Case Stud. Chem. Environ. Eng. 4 (2021), 100149.
[10] S. Bousbih, E. Errais, R.B. Amar, J. Duplay, M. Trabelsi-Ayadi, F. Darragi, Elaboration and characterization of new ceramic ultrafiltration membranes from natural clay: application of treatment of textile wastewater, in: Conference of the Arabian Journal of Geosciences, Springer, 2018, pp. 195–198.
[11] A. Chougui, A. Belouatek, M. Rabiller-Baudry, Synthesis and characterization of new ultrafiltration ceramic membranes for water treatment, J. Water Proc. Eng. 30 (2019), 100620.
[12] B. Nandi, R. Uppaluri, M. Purkait, Preparation and characterization of low cost ceramic membranes for micro-filtration applications, Appl. Clay Sci. 42 (1–2) (2008) 102–110.
[13] J.S. Reed, Principles of Ceramics Processing, Wiley, New York, 1995.
[14] S.H. Park, Y.G. Park, J.-L. Lim, S. Kim, Evaluation of ceramic membrane applications for water treatment plants with a life cycle cost analysis, Desalination Water Treat. 54 (4–5) (2015) 973–979.
[15] C. Cozic, L. Picton, M.-R. Garda, F. Marlhoux, D. Le Cerf, Analysis of Arabic gum: study of degradation and water desorption processes, Food Hydrocolloids 23 (7) (2009) 1930–1934.
[16] ASTM, Standard Test Method for Water Absorption, Bulk Density, Apparent Porosity, and Apparent Specific Gravity of Fired Whiteware Products, ASTM International, 2006.
[17] O.A. Al-Harbi, M. Mujtaba Khan, C. Özgür, Improving the performance of silica-based crossflow membranes by surface crystallization for treatment of oily wastewater, J. Australian Ceram. Soc. 53 (2) (2017) 883–894.
[18] B. Achiou, H. Elomari, A. Bouazizi, A. Karim, M. Ouammou, A. Albizane, J. Bennazha, S.A. Younssi, I. El Amrani, Manufacturing of tubular ceramic microfiltration membrane based on natural pozzolan for pretreatment of seawater desalination, Desalination 419 (2017) 181–187.
[19] M. Mouiya, A. Bouazizi, A. Abourriche, A. Benhammou, Y. El Hafiane, M. Ouammou, Y. Abouliatim, S.A. Younssi, A. Smith, H. Hannache, Fabrication and characterization of a ceramic membrane from clay and banana peel powder: application to industrial wastewater treatment, Mater. Chem. Phys. 227 (2019) 291–301.
[20] W.E. Federation, Membrane Systems for Wastewater Treatment, McGraw-Hill Education, 2005.
[21] J. Nayak, J. Bera, Effect of sintering temperature on phase-formation behavior and mechanical properties of silica ceramics prepared from rice husk ash, Phase Transitions 82 (12) (2009) 879–888.
[22] G. Anbalagan, A. Prabakaran, S. Gunasekaran, Spectroscopic characterization of Indian standard sand, J. Appl. Spectrosc. 77 (1) (2010) 86–94.
[23] C.O. Mgbemena, N.O. Ibekwe, R. Sukumar, A.R. Menon, Characterization of kaolin intercalates of oleochemicals derived from rubber seed (Hevea brasiliensis) and tea seed (Camelia sinensis) oils, J. King Saud Univ. Sci. 25 (2) (2013) 149–155.
[24] K. Bahranowski, A. Klimek, A. Gawel, E.M. Serwicka, Rehydration driven Na-activation of bentonite—evolution of the clay structure and composition, Materials 14 (24) (2021) 7622.
[25] A. Lesbani, P. Tamba, R. Mohadi, Fahmariyanti, Preparation of calcium oxide from Achatina fulica as catalyst for production of biodiesel from waste cooking oil, Indonesian J. Chem. 13 (2013) 176–180, https://doi.org/10.22146/ijc.21302.
[26] N. Elhadiri, M. Bouchdoug, M.b. Benchanaa, Valorization of powdered marble as an adsorbent for removal of methylene blue using response surface methodology, Appl. J. Environ. Eng. Sci. 5 (1) (2019) 53–65, 5-1 (2019).
[27] O. Mountoumnjou, A. Szymczyk, E.E. Lyonga Mbambyah, D. Njoya, A. Elimbi, New low-cost ceramic microfiltration membranes for bacteria removal, Membranes 12 (5) (2022) 490.
[28] N. Damayanti, Preparation of superhydrophobic PET fabric from Al2O3–SiO2 hybrid: geometrical approach to create high contact angle surface from low contact angle materials, J. Sol. Gel Sci. Technol. 56 (1) (2010) 47–52.
[29] S. Husain, Effect calcination temperature on formed of calcium silicate from rice husk ash and snail shell, Jurnal Neutrino:Jurnal Fisika dan Aplikasinya 11 (2) (2020) 45–51.
[30] G. Shao, X. Wu, Y. Kong, S. Cui, X. Shen, C. Jiao, J. Jiao, Thermal shock behavior and infrared radiation property of integrative insulations consisting of MoSi2/borosilicate glass coating and fibrous ZrO2 ceramic substrate, Surf. Coating. Technol. 270 (2015) 154–163.
[31] B. Achiou, H. Elomari, M. Ouammou, A. Albizane, J. Bennazha, A. Aaddane, S. A. Younssi, I.E.A. El Hassani, Study of added starch on characteristics of flat ceramic microfiltration membrane made from natural Moroccan pozzolan, J. Mater. Environ. Sci. 9 (2018) 1013–1021.
[32] F. Bouzerara, S. Boulanacer, A. Harabi, B. Boudaira, S. Achour, S. Condom, Preparation and characterization of macroporous ceramic supports for membranes, Phys. Procedia 2 (3) (2009) 1449–1453.

[33] S. Gautam, D.R. Cole, Effects of pore connectivity and tortuosity on the dynamics of fluids confined in sub-nanometer pores, Phys. Chem. Chem. Phys. 24 (19) (2022) 11836–11847.
[34] A. Ivanets, A. Rat, T. Azarova, S. Azarov, S. Al-Khowaiter, O. Al-Harbi, S. Shemchonok, V. Dobysh, V. Tarasevich, V. Agabekov, Preparation and properties of microfiltration membranes based on natural crystalline SiO2, Ceram. Int. 40 (8) (2014) 12343–12351.
[35] W. Wan, C.-e. Huang, J. Yang, J. Zeng, T. Qiu, Effect of sintering temperature on the properties of fused silica ceramics prepared by gelcasting, J. Electron. Mater. 43 (7) (2014) 2566–2572.
[36] M.B. Ali, N. Hamdi, M.A. Rodriguez, K. Mahmoudi, E. Srasra, Preparation and characterization of new ceramic membranes for ultrafiltration, Ceram. Int. 44 (2) (2018) 2328–2335.
[37] K. Lindqvist, E. Lidén, Preparation of alumina membranes by tape casting and dip coating, J. Eur. Ceram. Soc. 17 (2–3) (1997) 359–366.
[38] S. Diana, R. Fauzan, N. Arahman, F. Razi, E. Elfiana, Synthesis and Characterization of Microfiltration Ceramic Membrane Based on Fly Ash and Clay Mixture Using Sintering Method, IOP Conference Series: Materials Science and Engineering, IOP Publishing, 2020, 012019.